Acta Cryst. (1969). A**25**, 569

Dynamical Calculation of Thermal Diffuse Electron Scattering

BY P. A. DOYLE

School of Physics, University of Melbourne, Australia

(*Received* 21 *October* 1968)

The theory of Cowley & Pogany (*Acta Cryst.* (1968) A**24**,1 09) is used for the numerical calculation of thermal diffuse electron scattering from thin monatomic crystals, along the line of a set of systematic reflexions. Dynamical interactions of 15 Bragg and 25 diffuse beams are considered for up to 183 Å of gold (200) systematics, treating the range of coherence of the interaction as a parameter of calculation. A one-phonon Debye model is used. It is found that thermal diffuse scattering will not produce strong thickness fringe contrast, but will yield Kikuchi bands and lines, with little dependence on the range of coherent interaction. The unindexed Kikuchi line at the centre of the bands is predicted. Thermal scattering tends to increase in the region of strong Bragg beams for tilted crystals. Compared to that predicted kinematically, dynamical thermal scattering is greater for thin crystals near principal orientations, but will in general be less for highly tilted and particularly for thick crystals; it is more spread out in the diffraction pattern, and far stronger in the first Brillouin zone. There is an indication that thermal streak patterns from thin crystals should be stronger than expected kinematically.

Introduction

The kinematic theory cannot predict the intensities of Bragg beams with any accuracy in electron diffraction, because of their strong coupling. This is equally true for diffuse scattering, for even though it is normally weaker, it is generated from Bragg beams, and interacts (with itself) just as strongly. Thus, in order to study the contrast expected in imaging thermal background in electron microscopy, or the structure in the diffraction pattern, dynamical interaction of diffuse waves must be considered.

Theories treating thermal diffuse scattering (TDS) have been developed in varying degrees of approximation. Hall & Hirsch (1965) treated the Bragg beams as Bloch waves, by the two beam theory, and the TDS as plane waves. This approach was useful in explaining anomalous absorption, but could not give the detailed distribution of TDS. The work was extended from an Einstein model to a one-phonon and approximate many-phonon Debye model by Hall (1965). Yoshioka & Kainuma (1962) used the fundamental equations for dynamical diffuse scattering developed by Yoshioka (1957) to study thermal absorption from elastic waves, again ignoring the interaction of diffuse waves when considering specific cases. Alternative theories, with the use of a weak beam approach or time-independent perturbation methods, have been formulated by several workers (Kainuma & Yoshioka, 1966; Fukuhara, 1963; Kainuma, 1965).

Takagi (1958*a*,*b*) included dynamical interaction of diffuse waves, and in the case of two waves in thick crystals showed that TDS can form Kikuchi patterns. The work of Fujimoto & Kainuma (1963) extended this to thin crystals. Gjønnes (1966) considered diffuse waves as N-beam dynamic, assuming incoherent diffuse scattering from each region of crystal. He achieved a qualitative description of the profiles of Kikuchi lines and bands, but was limited quantitatively by omitting interference between diffuse waves produced at different depths in the crystal. O'Conner (1967) has treated TDS for X-rays and neutrons on a two-beam dynamical theory. It is the purpose of the present paper to discuss the intensity of TDS along a systematic line, when no non-systematic Bragg beams are appreciably excited, taking account of the effects of N-beam interaction and of partial coherence. To this end, numerical calculations have been performed based on the theory of Cowley & Pogany (1968).

Range of coherence of diffuse scattering processes

By the time an electron microscope beam reaches the specimen the wave packet of one electron has spread over a region large in dimensions compared with the crystal thickness. Taking the probability amplitude of finding the electron at any point in the crystal at a given time as constant is therefore a good approximation; elastic scattering of this wave packet can then only be localized within the crystal, so it is coherent. Similarly, when the scattering is inelastic, wave amplitudes, rather than intensities, should be added over the range to which the interaction can be localized.

The excitation of a collective vibration in the conduction electrons (a plasmon) is coherent typically over several hundred Ångströms. This is seen most easily by considering values of the velocity and relaxation time for plasmons. Experimental measurements by several workers (see Ehrenreich & Philipp, 1962) have confirmed that plasmon path-lengths are of this order. Coupled with the small energy and momentum transfers involved, this long coherence-length accounts for the similarity in the image produced from plasmon scattering and from Bragg beams (Howie, 1963).

For the creation or annihilation of a phonon, the range of coherent interaction between diffuse waves is the length of the phonon in the incident beam direction. Neutron diffraction line broadening experiments suggest that this can be shorter than one wavelength for short wavelength optical phonons above the Debye temperature (Brockhouse, 1964). For long wavelength acoustical phonons, it will extend over far greater distances. The present work treats the range of correlation as a parameter of calculation, to determine its importance for dynamical TDS.

Theory

Since we will calculate TDS for the systematics case only, the crystal structure in the y direction can be suppressed. If $\varphi_{0l}(x)$ is the potential of an atom at x_l, averaged over y and projected in the z direction over a crystal slice of thickness Δz, then the scattering function $q(x,z,t)$ for this slice can be written, following Cowley & Pogany (1968), as

$$q(x,z,t)=1+\exp\{\sum_n\sum_l i\sigma\varphi_{0l}(x)*\delta(x-x_l)*\delta[x-na-\Delta_{nl}(z,t)]\}-1\,. \quad (1)$$

Here, $\sigma=\pi/\lambda_0 W_0$, λ_0 and W_0 being the wavelength and accelerating voltage for the incident electron. $\Delta_{nl}(z,t)$ is a continuous function whose value at the position of an atom describes its displacement from equilibrium. Equation (1) assumes a rigid ion model for the vibrating atoms.

If there is no overlap of the $\varphi_{0l}(x)$ for different atoms, (1) can be written as

$$q(x,z,t)=1+\sum_n\sum_l[\exp\{i\sigma\varphi_{0l}(x-x_l)\}-1]*\delta[x-na-\Delta_{nl}(z,t)]\,. \quad (1')$$

Fourier transforming (1′) with respect to x,

$$F(u,z,t)=\delta(u)+\sum_n\sum_l F_{1l}(u)\exp(2\pi iux_l)\times\exp(2\pi iuna)\exp[2\pi iu\Delta_{nl}(z,t)], \quad (2)$$

where

$$F_{1l}(u)=\mathscr{F}[\exp\{i\sigma\varphi_{0l}(x)\}-1].$$

Equation (2) is the same as in kinematic theory for a single unit-cell layer, apart from the replacement of kinematic scattering factors by $F_{1l}(u)$. Therefore, following kinematic theory [see Cochran (1963)], Bragg beams are given by

$$F(u)=\sum_h\sum_l F_{1l}(u)\exp[-B_l(u/2)^2]\exp(2\pi iux_l)\times\delta(u-h/a)=\sum_h\sum_l F^T_{1l}(u)\exp(2\pi iux_l)\,.\,\delta(u-h/a)\,, \quad (3)$$

where the B_l's are the usual Debye–Waller factors.

In the case of one atom per fundamental cell, for which the question of the overlap of the $\varphi_{0l}(x)$ is irrelevant, $\Delta_n(z,t)$ can be written as

$$\Delta_n(z,t)=\sum_{js}A_{jsx}(t)\cos[k_{jx}na+k_{jz}z-\omega_{js}t+\alpha_{js}]\,. \quad (4)$$

$A_{jsx}(t)$ is the x component of the vibrational amplitude of the mode s with wave vector components $k_{jx}=2\pi/\lambda_{jx}$ and $k_{jz}=2\pi/\lambda_{jz}$. The phonons have energy $\hbar\omega_{js}$ and a phase factor α_{js}, taken as random. In this monatomic case, summations over l and the term $\exp(2\pi iux_l)$ are dropped, yielding for Bragg beams the simple expression

$$F(u)=\sum_h F^T_1(u)\delta(u-h/a)\,. \quad (3')$$

By expanding the last exponential in (2) as a product of a series of Bessel functions, Cowley & Pogany showed that (3′) is accurate to terms of fourth order in the small quantities (uA_{jsx}). Their expansion of (2) into terms corresponding to Bragg reflexion and to single and multiple-phonon single-scattering processes yielded, for the single phonon term, the approximate expression

$$F^D_1(u,z,t)=F^T_1(u)\sum_{js}\pm i\pi uA_{jsx}(t)\exp[\pm i(\alpha_{js}+k_{jz}z-\omega_{js}t)]\sum_h\delta(u-h/a\pm 1/\lambda_{jx})\,. \quad (5)$$

Multiple diffuse scattering is absent from this approximation; it will be negligible within the crystal thicknesses considered in this paper.

The time dependence of $A_{jsx}(t)$ is the result of statistical fluctuation of the number of phonons in the mode (js), and possibly of a slow increase resulting from heating of the crystal. Particularly since they are averaged in an experiment, both these small effects are ignored, $A_{jsx}(t)$ being replaced by $A^{(\mathrm{r.m.s.})}_{jsx}$, its root-mean-square value. Since $\omega_{js}\ll\omega_{el}$, the phase term $\exp(\pm i\omega_{js}t)$ varies little during the interaction, and so is eliminated when finding intensities. The random phases α_{js} mean that the observed intensity is a sum only of incoherent contributions from different phonons, since the time average of cross terms will be zero.

The $\pm$ signs in (5) are a result of taking a cosine form for vibrations, as in (4). They may be treated by doubling the final intensity predicted by either one. Thus the one-phonon diffuse scattering amplitude at a depth z in the crystal may be written, dropping the plus sign, as

$$F^D_1(u,z)=\sum_{js}F^D_1(u,z)_{js}\exp(-i\alpha_{js})\,,$$

where

$$F^D_1(u,z)_{js}=-i\pi uF^T_1(u)A^{(\mathrm{r.m.s.})}_{jsx}\times\exp(-ik_{jz}z)\sum_h\delta(u-h/a-1/\lambda_{jx})\,. \quad (6)$$

A quantum-mechanical treatment of dynamical thermal electron scattering would yield the same final intensities as the classical theory above, within minor approximations. This is readily seen by comparing (2)

with the work of Laval (1958) dealing with kinematic X-ray phonon scattering.

Method of calculation

(1) *Bragg beams*

Bragg beams are calculated by the iterative 'slice' approach of Goodman & Moodie (1965), as described by Cowley & Pogany (1968). This gives the elastic waves $F_N(h)$ at the Nth layer of crystal as

$$F_N(h)=\sum_{h_1} F_{N-1}(h_1)F_1^T(h-h_1)T(h-h_1)P(h_1,\beta)\,, \quad (7)$$

where the phase term $T(h)$ resulting from a crystal tilt β in the xz plane is

$$T(h)=\exp\left[\frac{-2\pi i\Delta z\tan\beta}{a}(N-1)h\right]$$

and that due to propagation of the waves between slices Δz apart, $P(h,\beta)$, is

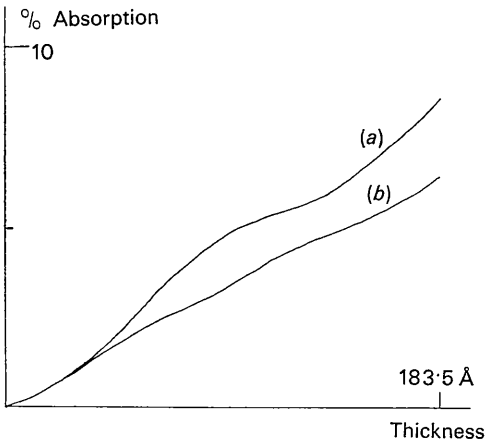

Fig. 1. Percentage absorption from Bragg beams against thickness, resulting from TDS for (200) gold systematics. (*a*) Zero tilt, (*b*) β=first Bragg angle.

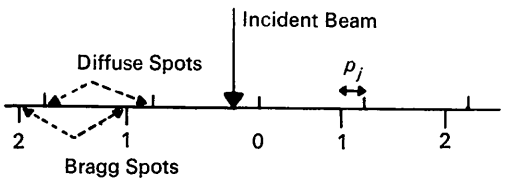

Fig. 2. Equivalent diffuse position in the diffraction pattern.

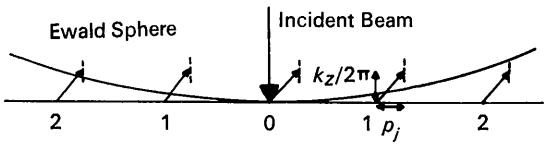

Fig. 3. Scattering power of wave vector (k_{jx},k_{jz}). --- Spread of diffuse scattering power.

$$P(h,\beta)=\exp\left[\frac{-i\pi\lambda\Delta z h^2}{a^2\cos^3\beta}\right].$$

From the derivation of (3′) it is clear that the use of a large slice thickness forces several fundamental cells to vibrate in phase, and so produces an overestimate of thermal absorption. Thus in calculating Bragg beams with absorption on the slice approach by the use of (7), single atom layers must be used. Fig. 1 shows the percentage of the incident beam lost from Bragg beams through thermal absorption for two tilts of (200) gold systematics, taking B=0·50 Å^2.

(2) *One-phonon diffuse beams*

The following describes the method employed to account for the interaction, on the systematic line, of diffuse beams caused by a single acoustical phonon. This allows the range of coherence to be varied arbitrarily.

The diffuse amplitude $F_1^D(u,z)_{js}$ corresponding to one vibrational mode is given by (6). For a set of Bragg beams $F_{N-1}(h)$ entering the Nth slice of crystal, the diffuse scattering produced by the mode (js) is

$$F_N^D(h+p_j,z_N)_{js}=\sum_{h_1} F_{N-1}(h_1)F_1^D(h-h_1+p_j,N\Delta z)_{js} \times T(h-h_1+p_j)P(h_1,\beta)\,, \quad (8)$$

where

$$p_j=a/\lambda_{jx}\,.$$

Equation (8) implicitly ignores multiple diffuse scattering. Multiple-phonon single scattering processes are omitted by the use of (6) for F_1^D.

The Bragg interaction, at later layers, of the diffuse waves produced at a depth $N_0\Delta z$ is given by the iteration

$$F_N^D(h+p_j,N_0\Delta z)_{js}=\sum_{h_1} F_{N-1}^D(h+p_j, N_0\Delta z)_{js}F_1^T(h-h_1)T(h-h_1)P(h_1+p_j,\beta-\Delta\beta) \quad (9)$$

where

$$\Delta\beta=\lambda/\lambda_{jx}\,.$$

Equation (9) is first applied at layer $N=N_0+1$, and includes absorption from one-phonon diffuse waves. It can be shown that the choice of terms P and T in (8) and (9) expresses the phases of diffuse waves relative to the central Bragg beam, as is the case for the Bragg beams. This allows additional TDS to be produced at layer N_0 with the correct relative phase. Choosing a particular λ_{jx}, appropriate to a phonon propagating in the $x-z$ plane, Bragg interactions of diffuse waves occur between specific diffuse points on the systematic line, themselves separated by reciprocal lattice vectors (Fig. 2).

In the calculation, Bragg beams are first calculated and stored for each layer of the crystal. Then, by the use of (8) and (9), the amplitudes and phases of diffuse waves at the diffusely scattering slice and each later slice of the crystal, up to the maximum desired thick-

ness, are calculated and stored. This is done considering each slice in turn as the source of thermal scattering. It is convenient to omit the term $A_{jsx}^{(\mathrm{r.m.s.})} \exp(-ik_{jz}z)$, then include it at the end of the crystal, multiplying the diffuse amplitudes by the term appropriate to that depth of crystal at which they were produced. This is valid since this term does not depend on the indices h or h_1, and so will not alter the dynamical interactions. Since $uF_1^T(u)$ varies little, except in the first Brillouin zone, for modes having the same k_{jx} but different k_{jz}, the same set of diffuse waves can be used for all phonons with the same k_{jx}.

Taking the range of coherent interaction as being $L\Delta z$, then for a particular mode, diffusely scattered amplitudes at the end of the crystal produced in the first L slices are added (with the term $A_{jsx}^{(\mathrm{r.m.s.})} \exp(-ik_{jz}z)$ included), then added in intensity to those produced at the end of the crystal in the next L slices, and so on. A linear average is taken over the positions of coherent interaction. In this way, the intensity produced by a given phonon can be found as a function of its length in the incident beam direction.

An orthogonal set of polarization vectors is assumed for the vibrations, and a Debye model taken for the dispersion relation. Under these conditions, $A_{jsx}^{(\mathrm{r.m.s.})}$ is given by

$$\overline{A_j^2} = \sum_s \overline{A_{jsx}^2} = \frac{1}{2N_3\lambda^2\Delta z}\left\{\frac{h}{\pi^2\varrho v}\cdot\lambda j\right\}\coth\left(\frac{hv}{2KT\lambda j}\right). \tag{10}$$

Here, N_3 is the number of layers of fundamental cells in the z (or incident) direction, ϱ the crystal density, K is Boltzman's constant, T the absolute temperature and v the sound velocity in the crystal. The additional factor of 2, resulting from the omission of the plus sign from (5) as mentioned previously, is included. Equation (10) sums over the incoherent contributions from transverse and longitudinal modes. The result is the same as for a single mode in the $\mathbf{k}_x$ direction, since TDS along this systematic line results only from the projected atomic vibration in this direction.

For later reference, we note that the kinematic one-phonon diffuse amplitude from one fundamental cell layer and from the wave vector $\mathbf{k}_j$, under the same conditions, is given by

$$F_{\mathrm{kin}}^D(u) = i\pi A_{jk}^{(\mathrm{r.m.s.})} u f_0^T(u)$$

where

$$\overline{A_{jk}^2} = \frac{c}{2V^2N_3}\left\{\frac{h}{\pi^2\varrho v}\lambda_j\right\}\coth\left(\frac{hv}{2KT\lambda j}\right). \tag{11}$$

Here V is the volume of the fundamental unit cell, c is the spacing of single atom layers, and $f_0^T(u)$ the kinematic scattering length attenuated by the Debye–Waller factor.

The use of (6), (10) and (11) gives TDS expressed as a scattering probability, so that an integration over the whole diffraction pattern would yield the fraction of electrons scattered by one-phonon processes from the particular crystal considered.

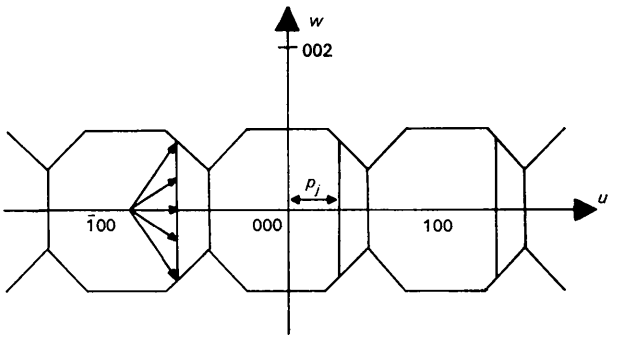

Fig. 4. The first Brillouin zone of the f.c.c. lattice down the [200] direction in reciprocal space. Only contributions from wave vectors within the octagons are included.

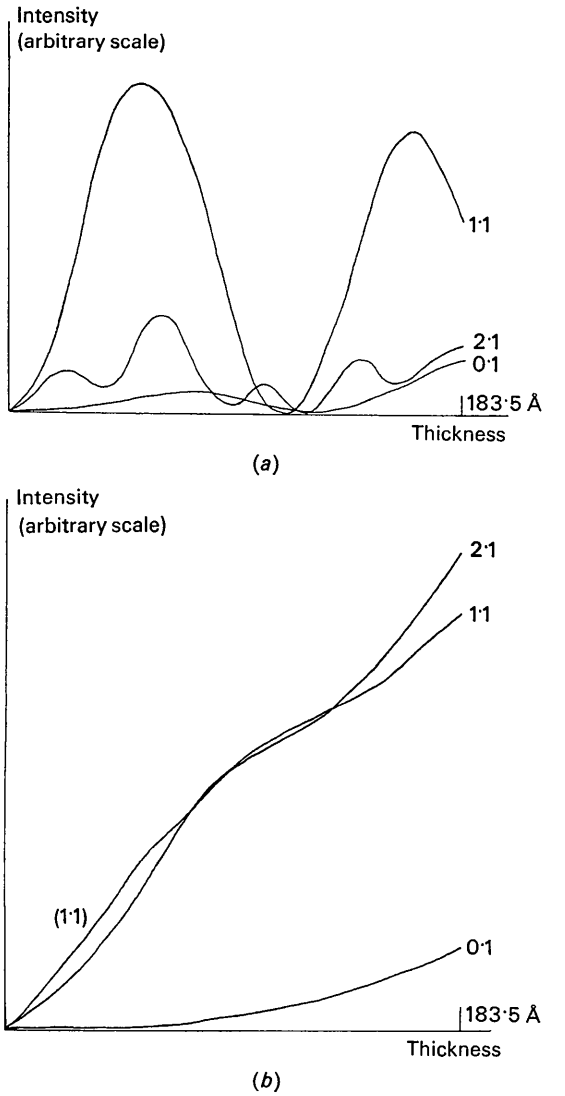

Fig. 5. Diffuse intensity plotted against thickness for zero tilt and the single mode defined by $p_j = 0{\cdot}1$, $k_{jz} = 0$, in the positions $(h+p_j) = 0{\cdot}1$, $1{\cdot}1$, $2{\cdot}1$. (*a*) Coherent case and (*b*) coherence length = 12·2 Å. For these two graphs only, $-\overline{A_j^2}$ was taken as an arbitrary constant, independent of thickness.

Calculations at this stage of development are not comparable to experiment, since contributions from different wave vectors are not resolved experimentally.

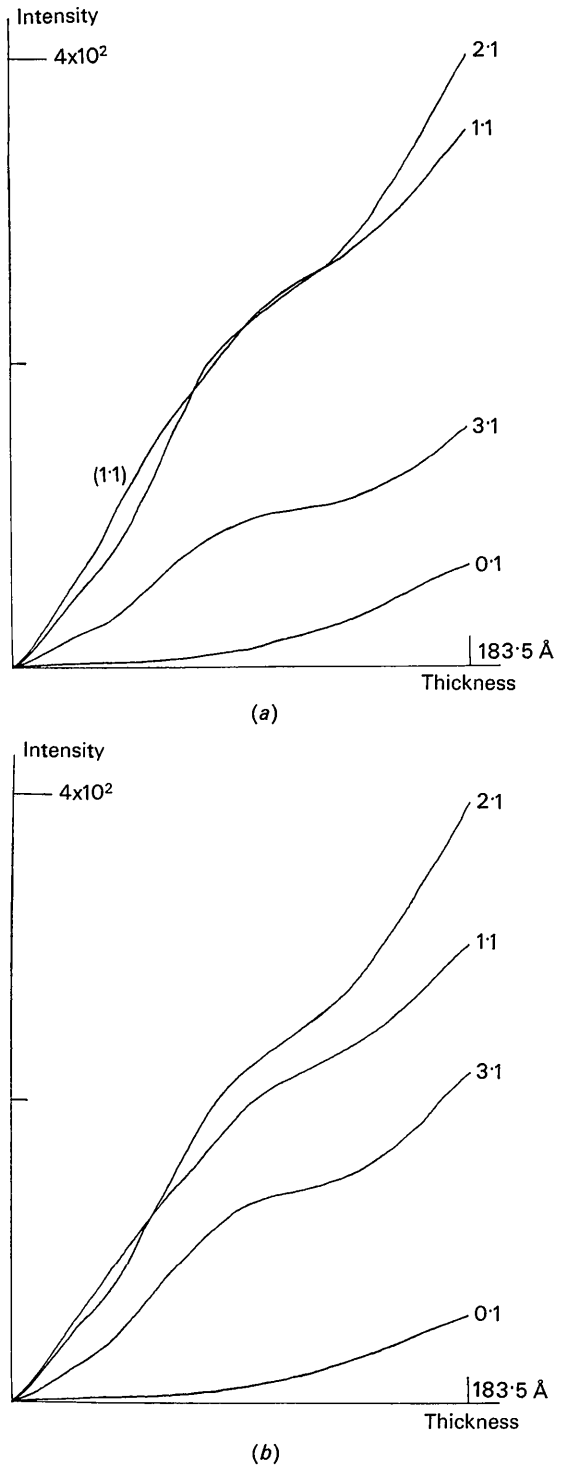

Fig. 6. As for Fig. 5, but including all modes with $p_j = 0{\cdot}1$. (*a*) Coherent case and (*b*) coherence length = 12·2 Å.

However, they show that the term $\exp(-ik_{jz}z)$ localizes the scattering power associated with a given wave vector, as shown in Fig. 3. Thus the thermal diffuse scattering power is envisaged as being composed of a set of dynamical shape functions centred on the allowed wave vectors, and smeared out by an amount which decreases with increasing coherence length and/or crystal thickness.

(3) *Coincident one-phonon contributions*

Experimentally, incoherent contributions to a set of diffuse positions separated by reciprocal lattice vectors, from modes having the same k_{jx} but different k_{jz}, are not resolved, so it is necessary to sum in intensity over allowed k_{jz} values for a given p_j. This is done by repeating, for each k_{jz}, the procedure outlined in the previous sub-section dealing with $A_{jsx}^{(\text{r.m.s.})} \exp(-ik_{jz}z)$.

The use of a set of normal modes to describe vibrations is strictly inconsistent with considering TDS as partially coherent, since both wave vectors and energies of phonons shift or smear out as the relaxation time decreases. It can be shown that this inconsistent step causes calculated TDS to double in going from a coherent to a completely incoherent case, even on a purely kinematic theory. This contradicts the well-known result that thermal absorption from Bragg beams is the same for an Einstein and for a Debye model. Therefore, it is necessary to renormalize the total intensity for partially coherent cases to equal that for the coherent case (for which the normal modes are strictly applicable), and to adjust each diffuse beam accordingly.

Fig. 4 shows the section of the first Brillouin zone for a face centred cubic crystal set down around each reciprocal lattice point in the [200] direction. Intensity contributions from wave vectors not included on this zero layer-line are omitted. Thus the present calculations cannot be performed for cases of such low coherence length that significant contributions to TDS on the systematic line would arise from these omitted wave vectors. The error introduced from this source in the cases considered is less than 10 per cent, and partially cancels when considering the dynamic factor as in the next section.

Because of the form of (6), diffuse beams spread further out in the diffraction pattern than do Bragg beams; therefore more diffuse beams must be considered in the interaction. In practice, 15 Bragg and 25 diffuse beams are found to be adequate for gold (200) systematics. A layer thickness Δz corresponding to three fundamental cells was used in treating interactions of diffuse waves, since it was found to introduce an error of no more than 5–10 per cent for diffuse beams in the first few zones.* Unfortunately, the length of the calculations is such that it must be limited to quite thin crystals – about 200 Å is an upper limit for gold. However, this is sufficient for our present purposes, and in any case calculations dealing with thick crystals would

* This was sometimes up to 15 per cent for the central zone.

have to treat multiple inelastic scattering processes (electronic as well as phonon excitation).

Calculated results

All calculations reported here are for gold (200) systematics, for crystals no greater than 183 Å thick, a temperature of 20 °C and an incident electron energy of 80 keV. Scattering factors calculated on the Dirac–Slater atomic model by Cromer & Waber (1965) were used to obtain atomic potentials. The difference between these and the relativistic Hartree–Fock values (Doyle & Turner, 1968) is not important considering other approximations in the present work.

(1) *Thickness contrast from TDS*

Fig. 5(*a*) and (*b*) show variation of diffuse intensity with thickness for the single mode defined by $p_j = +0{\cdot}1$ and $k_{jz}=0$ (as illustrated in Fig. 2), for assumed coherence lengths of infinity and 12·2 Å respectively.* These are for the untilted case, *i.e.* $\beta=0$. In the coherent case, turning points follow fairly closely those for the neighbouring Bragg beams, except for the central Brillouin zone. The different behaviour in this region may be a result of the weak direct contribution from the central beam. There is a monotonic increase with thickness for the low coherence case, as might be expected since the assumed coherence length is much less than typical Bragg beam extinction lengths for this graph.

As discussed previously in this paper, the diffuse intensity observed experimentally is a sum of incoherent contributions from wave vectors with different k_{jz} values. Figs. 6(*a*) and (*b*) correspond to Figs. 5(*a*) and (*b*), except that contributions from all modes are included. In both coherent and low coherence cases, little fringe-type variation is apparent, though it may be enhanced slightly by including absorption from electronic processes or by photographic techniques. This behaviour occurs for all tilts for the systematics case. It is consistent with the observations of Cundy, Metherall & Whelan (1966) who sought contrast from phonon scattered electrons from Al, and suggested that the observed contrast may be attributable to surface layers on the specimen.

The generally slower rate of increase of TDS at about 110–120 Å, apparent on Fig. 6(*a*) and (*b*), occurs because nearly all the elastic intensity is in the central beam at this thickness (the *N*-beam extinction length for the central beam in this case is 116 Å). The corresponding lower rate of absorption from Bragg beams at this thickness can be seen on Fig. 1 (curve *a*).†

(2) *Variation of intensity with coherence length*

It is often convenient to express results in terms of a dynamic factor *D*, defined as

$$D(L)=I_{\mathrm{dyn}}(L)/I_{\mathrm{kin}}\,. \qquad (12)$$

Here, I_{kin} is computed for coherent TDS, and is readily found by the use of (11), and summing over contributions from each mode as described in the dynamical case. In this way, effects resulting from partial coherence and dynamical interaction can be separated from those attributable to other causes, such as the model taken for vibrations.

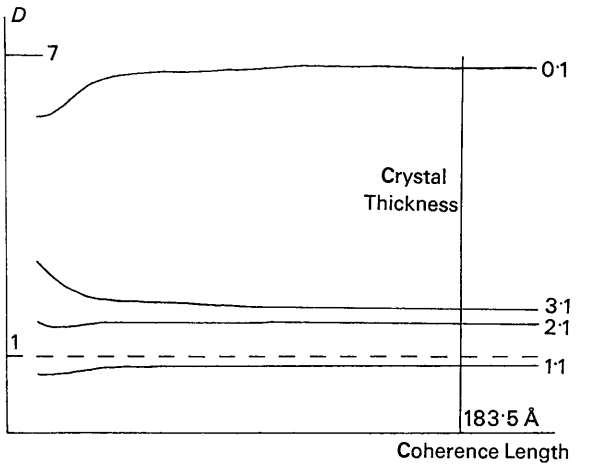

Fig. 7. The dynamical factor, *D*, plotted against coherence length, $L\Delta z$, for $\beta=0$ and $p_j=0{\cdot}1$, for a crystal 183 Å thick.

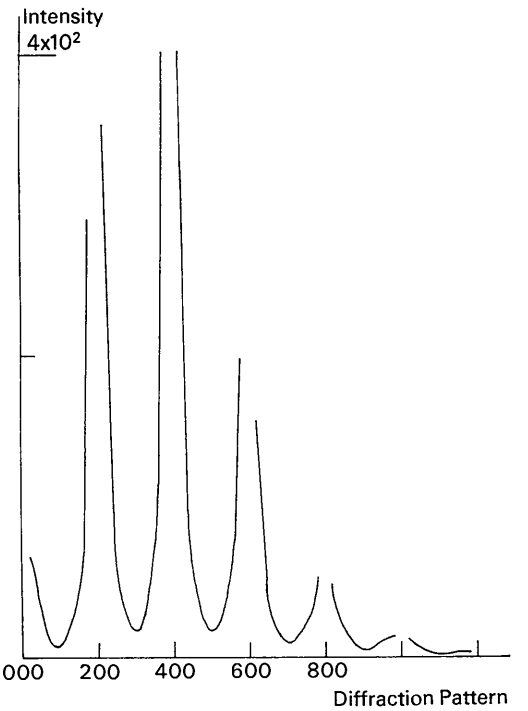

Fig. 8. Thermal diffuse scattering calculated across the diffraction pattern for 183 Å and $\beta=0$, coherent case.

* To retain consistency with the definition of p_j, the 200, 400, ... reflexions are denoted by $h=1, 2, \ldots$ on the graphs.

† *Note added in proof:* A more accurate treatment of thermal absorption would not predict this effect. However, further calculations have shown that the weak contrast in Fig. 6(*a*) and (*b*) is retained when the elastic intensity is exactly conserved, so that the above discussion remains valid. The prosent treatment of absorption does not have an important effect on any other calculations reported here.

Fig. 7 shows D against L for $\beta=0$, $p=0{\cdot}1$ and a thickness of 183 Å. The following points are noted:

(*a*) With the possible exception of the case of very low coherence diffuse intensity is almost independent of L. This is also found for other crystal tilts.

(*b*) Scattering in the first zone is far greater than that predicted kinematically. This is because normal processes are far less likely than Umklapp processes for phonon scattering, so that dynamical intensity in the first zone comes principally either directly from Bragg beams with $h\neq 0$, or through Bragg scattering of diffuse waves from other zones. Both these processes do not occur kinematically. This interpretation is borne out by noting that D for TDS in the first zone increases markedly with thickness, for any coherence length, a property not shared by TDS in other zones.

(*c*) D is in general greater than one, indicating stronger dynamical TDS than kinematic for this crystal. This is at first surprising since the same absorption function on Bragg beams is used in both cases. However, it is the difference between the kinematical and the effective dynamical shape functions surrounding each phonon wave vector which causes this effect. As crystal thickness increases, D will decrease, since, because intensity is conserved in the dynamical case, there is progressively less intensity in Bragg beams to 'feed' the diffuse scattering.

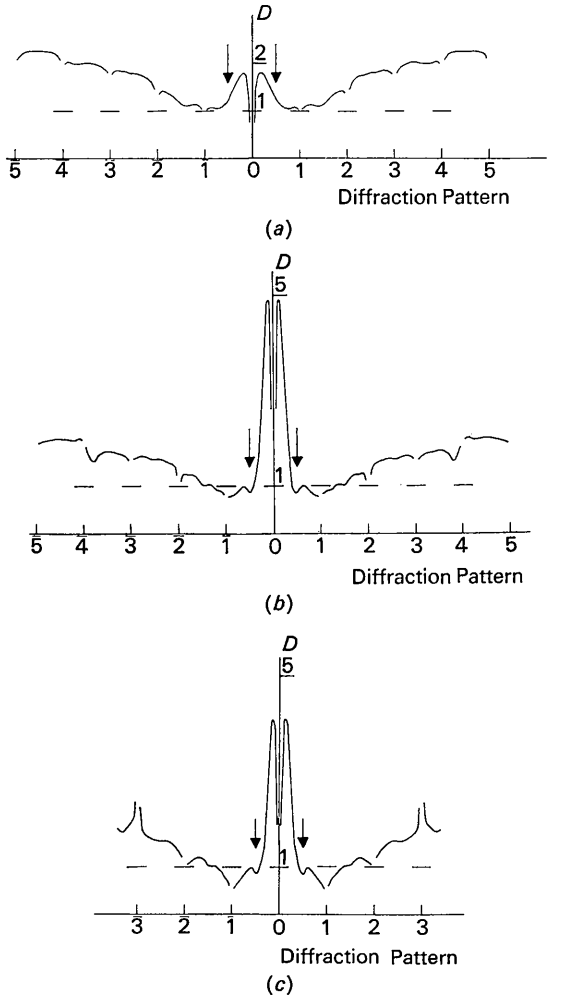

Fig. 9. The dynamical factor, D, plotted across the diffraction pattern for $\beta=0$. Arrows mark the limits of the Kikuchi band for 200 and $\bar{2}00$ reflexions. (*a*) Coherent, thickness = 92 Å; (*b*) coherent, thickness = 183 Å; (*c*) coherence length = 18·4 Å, thickness = 183 Å.

The coherence length is not an experimentally variable parameter (except partially by varying temperature), as are thickness, tilt and position in the diffuse background. For this reason, graphs with coherence as the independent variable are useful at this stage only for comprehension.

(3) *Structure in diffuse scattering*

It is well known that Kikuchi bands and lines in the background of diffraction patterns result from dynamical interaction of diffuse scattering. It has been suggested (Tonomura & Watanabe, 1967) that most intensity observed in these patterns is a result of scattering by electronic excitation (largely plasmon for certain substances). However, crystals which yield strong Kikuchi patterns are normally so thick that most electrons have suffered more than one inelastic scattering both thermal and electronic. Hence electrons scattered by phonons alone are not expected to contribute strongly to such Kikuchi patterns in terms of absolute intensity, as is found experimentally, but they may still possess the same structure on a smaller intensity scale.

Graphs of intensity across the diffraction pattern show little other than poles around each Bragg beam, resulting from the Debye model taken for vibrations. Fig. 8 shows such a graph for $\beta=0$. (TDS is symmetrical about the central spot in this case.) Graphs of D prove more useful, as in Fig. 9. The Kikuchi band for 200 and $\bar{2}00$ reflexions is expected to be symmetrically placed about the origin, as shown. It is not apparent at 92 Å [9(*a*)], but is becoming defined for 183 Å for both coherent and low coherence cases [9(*b*) and (*c*)]. As the crystal is tilted, the structure in graphs of this type follows the various Kikuchi line positions. Fig. 10(*a*) and (*b*) are for a tilt equal to the first Bragg angle. However, it is not clear whether this suggestion of Kikuchi lines is dependent on coherence length. To investigate this, graphs of the type shown in Figs. 6 and 7 (intensity *versus* thickness and D *versus* L) were calculated for various Kikuchi line positions. They showed no more structure than can be seen in Figs. 6 and 7. It therefore appears that TDS can form Kikuchi bands and lines, whether or not the coherence length for the interaction is long. This explains why the treatment of diffuse scattering as incoherent (Gjønnes, 1966) can give a qualitative description of the profiles of Kikuchi patterns in the case of TDS.

The tendency for D to decrease sharply close to the central spot in the untilted case (Fig. 9) is a result of the symmetry of the interaction for this tilt, together with

the antisymmetry of the diffuse scattering function ($uF_1^T(u)$). For the two-beam case (Fig. 10), TDS in the central zone is asymmetrical, being greater between the two strong Bragg beams. Experimentally, it is observed that the total diffuse scattering near these two beams is lower between them. However, Howie (1963) has shown that this effect is to be expected for plasmon scattering from thick crystals, an essential point being that Umklapp processes do not occur for plasmons. On his argument, TDS provides a strong 'inelastic interband' mechanism, and so would not produce the effect observed for the total diffuse scattering (which is largely plasmon for many crystals, particularly near the centre of the diffraction pattern). Therefore the present result does not contradict experiment. For a large tilt such as 2·6 θ_{200} (Fig. 11), the effect continues, D being in general large in the region of strongly excited Bragg beams. There is a marked increase from 92 to 183 Å [11(*a*) and (*b*)], but again little difference in the case of low coherence [11(*c*)].

There is an indication in Figs. 10(*a*) and (*b*) of the formation of an unindexed defect Kikuchi line at the centre of the bands for the systematics case. It is also apparent for other low tilts, but not for large tilts [*e.g.* 11(*b*)] for the thin crystals considered. Kainuma & Kogiso (1968) have also predicted this experimentally observed phenomenon for the approximation of 3 Bragg and 3 diffuse beams of unspecified origin.

Thermal streak patterns have been observed in electron diffraction from several substances [see Honjo, Kodera & Kitamura (1964)]. They are the result of large vibrational amplitudes for specific modes, and are not dependent for their appearance on dynamical effects. Therefore they have their counterpart in X-ray diffraction, in the form of non-radial streaks. There is no streak through the central spot, so that the present calculations, being limited to the systematic line, cannot be directly applied to their study. However, D is in general greater than one for thin crystals with low tilt. This suggests that thermal streak patterns from acoustical phonons in thin crystals may be stronger than expected kinematically, when observed near principal orientations. When they are the result of low frequency optical phonons (as in $BaTiO_3$) the present calculations cannot be even qualitatively applied.

Discussion

The principal conclusions of the previous section may be summarized as the following :

(*a*) TDS spreads out further in the diffraction pattern and is far stronger around the central spot, than is expected kinematically;

(*b*) TDS is greater than predicted kinematically for thin crystals close to principal orientations, but in general is less for highly tilted or particularly for thick crystals;

(*c*) thickness fringes from one-phonon diffuse scattering are expected to be weak, whether coherent or incoherent. This results from the averaging caused by summing over phonon wave vectors;

(*d*) TDS can form Kikuchi bands and probably also Kikuchi lines, including the unindexed line at the centre of the bands, with little dependence on the range of coherence and hence phonon path length;

(*e*) dynamical interactions of diffuse waves may increase the intensity of thermal streak patterns from acoustical phonons in untilted thin crystals;

(*f*) when an inner reflexion is satisfied TDS between two strong beams tends to be greater than elsewhere. This remains true in the region of strong Bragg beams when several are strongly excited.

In general, phonon path length, and therefore coherence length, increases as thermal resistivity and expansion coefficients decrease. Therefore, experiments to verify the present prediction of a small dependence of TDS on coherence length could perhaps be carried out by use of different crystals having a suitable range of these macroscopic parameters.

The quantitative accuracy of the type of calculation reported here is difficult to assess. In the case of one atom per fundamental cell, for which ignoring the overlap of the projected potentials of different atoms is irrelevant, the principal approximations used are these:

(*a*) Multiple phonon single scattering processes have been ignored. These will produce TDS further out in

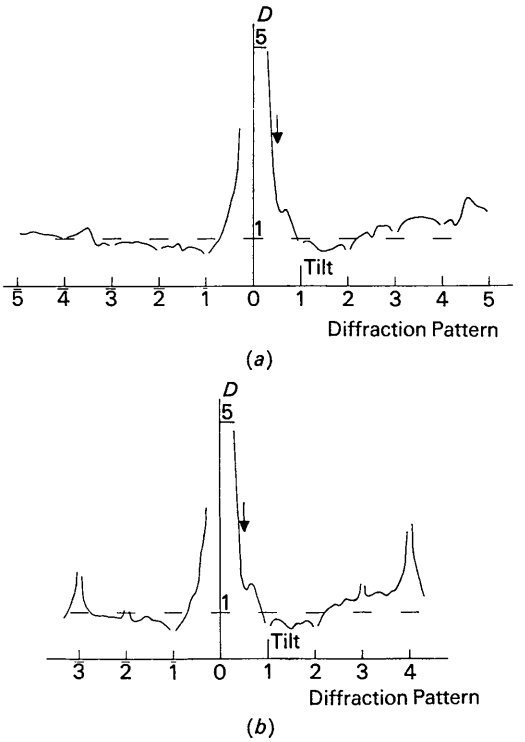

Fig. 10. The dynamical factor, D, plotted across the diffraction pattern for $\beta=\theta_{200}$, and 183 Å thickness, (*a*) coherent case and (*b*) coherence length = 18·4 Å. The arrow marks the position of the unindexed Kikuchi line.

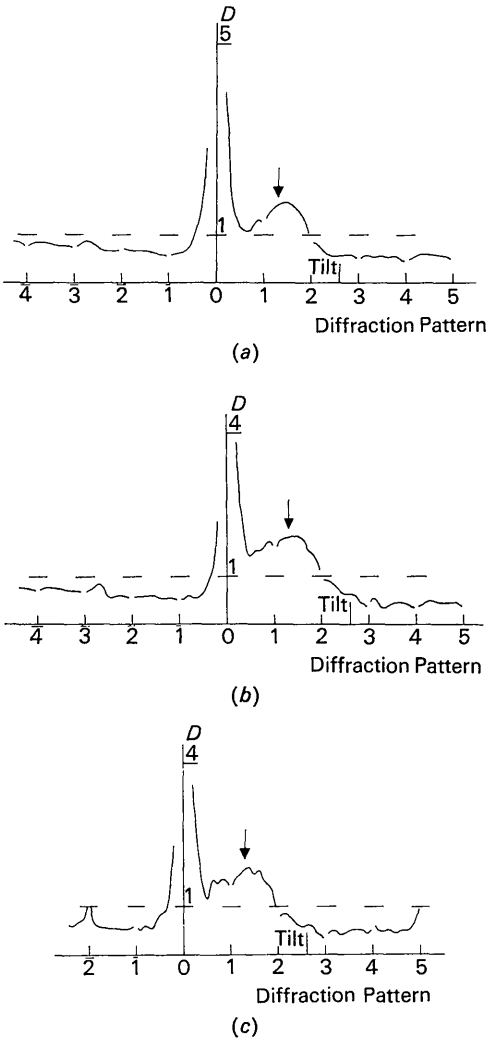

Fig. 11. The dynamical factor, D, plotted across the diffraction pattern for $\beta = 2{\cdot}6\theta_{200}$, and 183 Å thickness. (*a*) Coherent, thickness = 92 Å; (*b*) coherent, thickness = 183 Å; (*c*) coherence length = 18·4 Å, thickness = 183 Å.

the diffraction pattern than single-phonon scattering so that intensity in the first few zones may be mostly the result of single phonons. However, dynamical effects could well smear out electrons scattered by these processes to give appreciable contributions in the inner zones. This is probably the most serious approximation. The omission of the contribution resulting from multiple diffuse scattering, and the absorption resulting from electronic excitations, should not be important for the thin crystals considered.

(*b*) The Debye model taken for vibrational amplitudes could result in an important error for short wavelength modes, but this error cancels out to first order in considering the dynamic factor.

(*c*) Coherence length has been taken to be the same for all modes, whereas it should vary with wave vector and direction of the incident wave. The small dependence of the results on coherence length reduces the importance of this error.

(*d*) The systematics approximation is important for the case of gold – a truly systematics case does not seem possible for this crystal*. It was chosen for the present work because of the short Bragg beam extinction distances compared with those for a light element.

Unfortunately, the elimination of these and other less important approximations from calculations by use of the methods described appears to be impracticably difficult.

The author is indebted to Professor J. M. Cowley for his valuable suggestions and encouragement, and to Dr A. P. Pogany for many stimulating discussions. His thanks are also due to Dr P. S. Turner for permission to build on his computer program dealing with Bragg beam calculations. This work was supported by a research grant from the Australian Atomic Energy Commission.

References

Brockhouse, B. N. (1964). *Phonons and Phonon Interactions*. Ed. T. A. Bak. New York: Benjamin.
Cochran, W. (1963). *Rep. Prog. Phys.* **26**, 1.
Cowley, J. M. & Pogany, A. P. (1968). *Acta Cryst.* A**24**, 109.
Cromer, D. T. & Waber, J. T. (1965). *Acta Cryst.* **18**, 104.
Cundy, S. L., Metherall, A. J. F. & Whelan, M. J. (1966). Sixth International Congress on Electron Microscopy, Kyoto.
Doyle, P. A. & Turner, P. S. (1968). *Acta Cryst.* A**24**, 390.
Ehrenreich, H. & Philipp, H. R. (1962). *Phys. Rev.* **128**, 1622.
Fujimoto, F. & Kainuma, Y. (1963). *J. Phys. Soc. Japan*, **18**, 1792.
Fukuhara, A. (1963). *J. Phys. Soc. Japan*, **18**, 496.
Gjónnes, J. (1966). *Acta Cryst.* **20**, 240.
Goodman, P. & Moodie, A. F. (1965). *International Conference on Electron Diffraction and Crystal Defects*, Melbourne. ID-1, ID-2.
Hall, C. R. (1965). *Phil. Mag.* **12**, 815.
Hall, C. R. & Hirsch, P. B. (1965). *Proc. Roy. Soc.* **286**A, 158.
Honjo, G., Kodera, S. & Kitamura, N. (1964). *J. Phys. Soc. Japan*, **19**, 351.
Howie, A. (1963). *Proc. Roy. Soc.* **271**A, 268.
Kainuma, Y. (1965). *J. Phys. Soc. Japan*, **20**, 2263.
Kainuma, Y. & Kogiso, M. (1968). *Acta Cryst.* A**24**, 81.
Kainuma, Y. & Yoshioka, H. (1966). *J. Phys. Soc. Japan*, **21**, 1352.
Laval, J. (1958). *Rev. Mod. Phys.* **30**, 222.
O'Conner, D. A. (1967). *Proc. Phys. Soc.* **91**, 917.
Takagi, S. (1958*a*). *J. Phys. Soc. Japan*, **13**, 278.
Takagi, S. (1958*b*). *J. Phys. Soc. Japan*, **13**, 287.
Tonomura, A. & Watanabe, H. (1967). *Jap. J. Appl. Phys.* **6**, 1163.
Yoshioka, H. (1957). *J. Phys. Soc. Japan*, **12**, 618.
Yoshioka, H. & Kainuma, Y. (1962). *J. Phys. Soc. Japan*, **17**, Supp. BII, 134.

* The author is indebted to A. F. Moodie for pointing this out.